Dual-Color Nanoscale Assemblies of Structurally Stable, Few-Atom Silver Clusters, As Reported by Fluorescence Resonance Energy Transfer

Danielle Schultz,[†] Stacy M. Copp,[‡] Nemanja Markešević,[§] Kira Gardner,[‡] Sumant S. R. Oemrawsingh,[§] Dirk Bouwmeester,[‡,§] and Elisabeth Gwinn[‡,*]

[†]Chemistry and Biochemistry Department and [‡]Physics Department UCSB, Santa Barbara, California 93117, United States and [§]Huygens Laboratory, Leiden University, 2333 CA Leiden, The Netherlands

ABSTRACT We develop approaches to hold fluorescent silver clusters composed of only 10−20 atoms in nanoscale proximity, while retaining the individual structure of each cluster. This is accomplished using DNA clamp assemblies that incorporate a 10 atom silver cluster and a 15 or 16 atom silver cluster. Thermally modulated fluorescence resonance energy transfer (FRET) verifies assembly formation. Comparison to Förster theory, using measured spectral overlaps, indicates that the DNA clamps hold clusters within roughly 5 to 6 nm separations, in the range of the finest resolutions achievable on DNA scaffolds. The absence of spectral shifts in dual-cluster FRET pairs, relative to the individual clusters, shows that select few-atom silver clusters of different sizes are sufficiently stable to retain structural integrity within a single nanoscale DNA construct. The spectral stability of the cluster persists in a FRET pair with an organic dye molecule, in contrast to the blue-shifted emission of the dye.

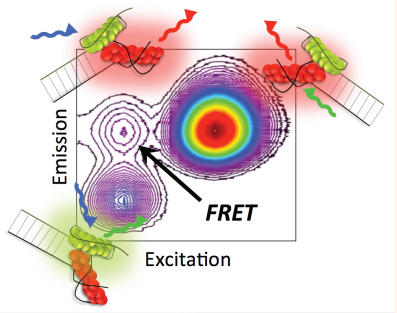

KEYWORDS: metal nanoclusters · fluorescent nanoclusters · DNA nanotechnology · FRET · nanocluster rods · fluorescent silver clusters

DNA self-assembly offers the opportunity to create nanostructures with unique optical properties that arise from the spatial organization of metal particles at length scales much smaller than visible light wavelengths. Recent efforts to exploit this potential used double-stranded DNA constructs to control near-field interactions in noble metal nanoparticle arrays,[1−5] resulting in modified optical phenomena such as visible-wavelength chirality and Fano-like resonances. Because fluorescence quantum yields are low (10^{-7} to 10^{-6}) for bulk-like metal particles with diameters of a few to tens of nanometers,[6] photon emission is difficult to detect. Instead, the spatial organization of metal particles by the DNA was reported by changes in photon absorption and scattering.[1−5]

As size is reduced from the bulk nanoparticle regime to the limit of quantum-size clusters with 10−20 atoms and dimensions of up to a few Fermi wavelengths, the availability of nonradiative decay paths falls and fluorescence quantum yields rise.[7,8] Thus, the organization of quantum-size metal clusters on DNA constructs has the potential to produce optical functionalities based on photon emission, rather than absorption or scattering, to report interactions that arise from near-field couplings. Fluorescence detection has numerous advantages, including intrinsically low background, high specificity, and availability of sophisticated techniques for single emitter detection and for direct imaging at length scales down to ∼10 nm.

Producing such small metal clusters in aqueous solution requires the use of stabilizing ligands to prevent agglomeration. Fluorescent clusters of silver have been realized using a variety of ligands,[9] including dendrimers,[10] peptides,[11] and polymers.[12] Fluorescent silver clusters have also been stabilized by small molecules such as thiols,[13]

* Address correspondence to bgwinn@physics.ucsb.edu.

Received for review June 28, 2013 and accepted October 3, 2013.

Published online October 03, 2013
10.1021/nn4033097

glutathione,[14] and dihydrolipoic acid[15] as well as in microemulsions.[16] Particularly promising are silver clusters stabilized by DNA oligomers.[17] Recent work has demonstrated that monodispersed clusters with fluorescence quantum yields close to unity[18,19] can be isolated for sizes ranging from 10 to 20 silver atoms when these clusters are stabilized by suitably chosen DNA sequences. The ability to separate DNA-wrapped clusters that differ in cluster size by just one metal atom is essential to controlling optical properties: contrary to 10 nm metal nanoparticles, which contain $\sim 10^4$ to 10^5 atoms,[20] and are consequently insensitive to single atom changes in size, metal clusters at the 10 atom size scale exhibit significant changes in optical properties with addition or subtraction of just one atom.[21,22]

Emerging applications for DNA-stabilized, fluorescent silver clusters include fluorescence signaling of target strands,[23−26] biosensors based on photoinduced electron transfer,[27] and logic devices that employ ion-tuned fluorescence.[28] The ability to tune silver cluster color throughout the visible and near-IR spectrum using sequence modification[8,29−31] is a unique feature that makes silver clusters particularly promising candidates for photonic elements within DNA-based, nano-optical structures. An order of magnitude smaller than semiconductor quantum dots, the 1−2 nm hydrodynamic radii of DNA-stabilized silver clusters[32] would permit incorporation into DNA scaffolds at spacings that fully exploit the high resolution positioning attainable through current techniques of DNA nanotechnology.[33−36] Select oligomers have been shown to template silver clusters that are more photostable than high quality organic dyes,[37] facilitating detection of the emission spectra from individual silver clusters.[38] Lastly, the high polarization dependence of silver cluster emission, which appears to arise from a rod-like cluster structure,[18] is promising for realization of directional information processing along DNA-based optical arrays.

Despite these unique features of DNA-stabilized silver cluster emitters, there is no evidence that such few-atom metal clusters can actually be assembled within nanoscale proximity. DNA nanotubes have been decorated with silver cluster emitters that were stabilized by single-stranded DNA extrusions from the double-stranded tube scaffold, but the separation distance between clusters was large (~1000 nm), and each emitter was held in the same cluster-templating sequence.[39]

Here we focus on assembling clusters of *different* size at 100 times smaller separations. Achieving such multicluster, nanoscale constructs is a challenging goal for DNA nanotechnology. For bare silver clusters, size-dependent free energies and electrochemical potentials[40,41] tend to drive structural reorganization of different sized clusters in an aqueous environment. The interaction of silver clusters with the DNA bases might, in principle, provide stability. However, solutions containing various DNA-stabilized silver clusters of unknown composition exhibited changes in fluorescence color and brightness when mixed with additional DNA oligomers,[42,43] indicating that the initially formed clusters were structurally altered when the overall DNA surroundings changed.

These results raise the question of whether silver clusters of different size, held in their particular DNA templates, can remain stable when brought together into one nanoscale construct, a step that necessarily alters the DNA environment. Currently, this question cannot be answered from first principles because the mechanisms by which the DNA base composition sets the sizes and stabilities of fluorescent silver clusters are not understood.

Thus, whether DNA constructs can hold fluorescent silver clusters of different size at nanometer-scale separations is an open question that must be addressed in order to determine whether the unique properties of these clusters can be exploited in nanoscale, multicolor constructs. We approach this question by seeking to form bicolor, dual cluster assemblies using clusters with spectral properties that would enable Fluorescence Resonance Energy Transfer (FRET) if each silver cluster of different size retained its structural integrity.

In FRET,[44,45] an excited "donor" fluorophore transfers energy nonradiatively to a nearby "acceptor"" fluorophore, which then emits a photon. The signature of FRET is emission from the acceptor (A) for excitation of the donor (D). FRET requires donor and acceptor to be at separations less than or comparable to a characteristic length scale, R_0, which depends on the spectral overlap of the donor emission spectrum with the acceptor absorbance spectrum. Since the underlying resolution of DNA scaffolds is typically 5−10 nm, testing whether silver clusters can be arrayed at length scales that exploit this resolution requires stable donor and acceptor clusters for which R_0 is in the 5−10 nm range. Here we design nanoscale DNA assemblies to incorporate such clusters and establish that select clusters exhibit both the requisite spectral properties for FRET and the requisite structural stability to enable assembly into a single, nanoscale construct.

Figure 1 shows schematics for the dual cluster assembly designs. In each case, the green and red cartoons represent the donor (D; green) and acceptor (A; red) clusters, which are held within their respective DNA templates. The double-clamp (DC) assembly flanks these templates with complementary regions designed to clamp the clusters together at both ends. The single-clamp (SC) assembly holds the clusters together at just one end, on the same side of the hybridization clamp. The end-to-end (EE) assembly places the cluster templates at opposite ends of the clamp. The hybridization tails are sequences of A and T bases, with 13 bases for each of the two tails in the DC assembly, and 30 bases in the SC and EE assemblies (sequences are listed in Materials and Methods).

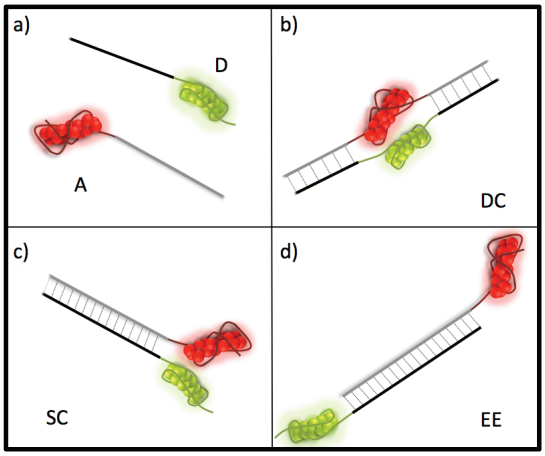

Figure 1. Designs for the desired dual cluster assemblies. (a) Cartoons of the individual DNA-stabilized donor (D) and acceptor (A) silver clusters. Distinct cluster-templating sequences, shown as wrapped around the clusters, select the cluster size and corresponding color. The extensions represent hybridization tail sequences. (b) The double clamp (DC) assembly design has complementary tails on both sides of the cluster-templating sequences. (c) The single clamp (SC) assembly design has hybridization tails on just one side of the cluster templating sequences. (d) The hybridization tails in the end-to-end (EE) assembly are designed to hold the clusters apart.

RESULTS AND DISCUSSION

To obtain unequivocal evidence for or against formation of the desired bicolor assemblies, our approach is to separately purify the DNA strand monomers that contain the donor and acceptor clusters and then to assemble the monomers into dual cluster constructs by hybridization of their complementary tails. This approach is necessitated by the heterogeneity of as-synthesized silver-DNA solutions. Prior work has shown that reduction of silver ions on DNA strands typically produces multiple fluorescent and nonfluorescent products that contain different numbers of silver atoms.[18,46] Because the color, Stokes shift, and chemical stability vary widely among these products, hybridizing the unpurified solutions typically produces multiple fluorescence peaks at wavelengths that shift over time, providing little insight into whether the desired construct forms as one of many possible hybridization products.

Use of homogeneous solutions containing sufficiently stable clusters of known size is key to the work presented here. We identify DNA templates that previous studies have found to produce silver clusters with good quantum yields that are also stable enough to purify and identify by high performance liquid chromatography with in-line mass spectrometry (HPLC-MS),[18] and that have spectral characteristics suitable for FRET. The selected donor, D, is a green emitting cluster (560 nm peak emission) containing 10 silver atoms in a 19-base DNA template, as previously established by mass spectrometry on the purified material.[18] The primary acceptor, A1 (670 nm peak emission), a 15 Ag atom red-emitting cluster in a 28 base template,[18] is used in all design schemes (DC, SC and EE). A second acceptor, A2 (635 nm peak emission), a 16 Ag atom cluster in a 22 base template,[18] is used in the SC scheme to test the generality of silver cluster FRET. The fluorescence quantum yields of these clusters are 40%, 75%, and 90% for D, A1, and A2, respectively.[18] All clusters are stable after HPLC isolation and reconcentration by spin filtration on time scales of several weeks to several months.

According to standard Förster theory,[44,45,47] the spectral overlap integral, donor quantum yield, and relative orientations of the transition dipole moments of D and A determine the Förster distance, R_0:

$$R_0^6 = \frac{9\ln(10)Q_0\kappa^2\left(\int f_D(\lambda)\varepsilon_A(\lambda)\lambda^4 d\lambda\right)}{128\pi^5 n^4 N_A} \quad (1)$$

Here, Q_0 is the donor fluorescence quantum yield, n is the index of refraction (1.33 for water), f_D is the donor emission spectrum normalized to unity integral over wavelength λ, ε_A is the extinction spectrum of the acceptor in SI units (cm^2/mol), N_A is Avogadro's number, and κ^2 is a unitless factor describing the relative orientation of donor and acceptor.

The FRET efficiency,

$$E_{FRET} = 1/[1 + (r/R_0)^6] \quad (2)$$

gives the probability that excitation of the donor will result in emission from the acceptor, where r is the separation between the D and A silver clusters. For $r = R_0$, $E_{FRET} = 0.5$; efficiency decays rapidly for larger r. Because energy transfer to the acceptor reduces donor emission, E_{FRET} can be measured by comparing the peak emission intensity of the donor monomer, I_D, to the peak donor emission intensity from the D–A assembly, I_{DA}.[47] Assuming all donor clusters in solution are paired with acceptor clusters, the FRET efficiency is

$$E_{FRET} = 1 - I_{DA}/I_D \quad (3)$$

We note that fluorescence lifetime measurements can also be used to determine FRET efficiencies without assumptions about the fraction of donors paired to acceptors, if the lifetime difference between paired and unpaired donors is sufficiently large.[47] Here we present only intensity-based measurements.

Figure 2 shows the well-separated emission spectra (solid lines) and absorbance spectra (dashed lines) of the HPLC-purified solutions of the donor cluster D (green traces) and acceptor cluster A1 (red traces). Spectra for acceptor A2 are shown in Supporting Information (Figure S.1). For each D–A pair, the absorbance peak of the acceptor is significantly redder than the donor absorbance peak. Thus, excitation of the donor will not produce significant excitation of the acceptor, except in the case of FRET.

A significant overlap between donor emission and acceptor absorbance is also evident in Figure 2 and Supporting Information (Figure S.1) (illustrated by shaded

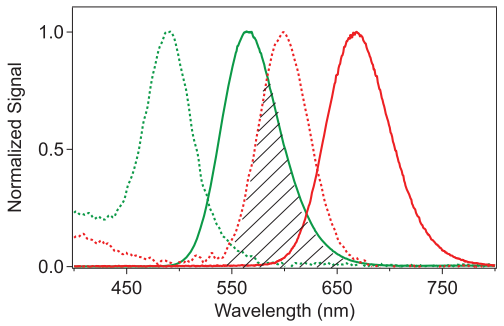

Figure 2. Normalized absorbance and emission spectra of donor D (green) and acceptor A1 (red) cluster. Dashed lines: absorbance. Solid lines: emission. The shaded region marks the range of spectral overlap between donor emission and acceptor absorbance.

region). R_0 values depend on this spectral overlap. We estimated visible extinction coefficients, ε_{vis}, of the clusters from absorbance spectra of the HPLC-purified solutions together with the fluorescence ($F_{\lambda max}$) and UV absorbance (A_{260}) chromatograms recorded during HPLC[46] (Supporting Information Figure S.2a), where $F_{\lambda max}$ is the fluorescence signal at the peak visible emission wavelength of the cluster.[18] Comparison of time-dependences of A_{260} and $F_{\lambda max}$ chromatograms provides an estimate of the purity after one round of HPLC. To estimate concentrations, we assume that A_{260} of the DNA-bound cluster is dominated by the DNA, as indicated by the similarity of UV spectra to the bare oligomers (Supporting Information Figure S.2b). It appears that high energy transitions of the clusters contribute relatively little to absorbance near 260 nm, where the DNA bases absorb strongly, as expected from calculations for atomic silver chains.[54,55] The purity-scaled A_{260} and the known DNA extinction coefficient of the strand provide the estimated concentration of the cluster, which together with the peak A_{vis} gives the peak visible extinction coefficient, ε_{vis}. We find ε_{vis} = $(0.9 \pm 0.2) \times 10^5$, $(1.4 \pm 0.2) \times 10^5$, and $(2.1 \pm 0.7) \times 10^5$ M^{-1} cm^{-1} for D, A1, and A2, respectively.

Because the orientations of the D and A clusters with respect to their DNA templates are unknown, we have no *a priori* knowledge of the orientation factor, κ^2. Thus, we included a flexible linker sequence of three to four T bases between the cluster templates and the hybridization sequences to promote orientational averaging of the relative transition moments of D and A clusters in the SC and EE assemblies. In the case of randomized transition moment orientations, $\kappa^2 = 2/3$. Using this standard orientation-averaged value gives R_0 values of 6.2 ± 0.2 and 6.7 ± 0.4 nm for D−A1 and D-A2, respectively. The same T-linkers were used at both ends of the cluster template sequences for the DC assembly, although in this case the constraints imposed by the double clamp will tend to reduce orientational freedom. If such constraints, or van der Waals or other interactions between the DNA-wrapped clusters, were to produce a net, time-averaged alignment of the transition dipoles, values for κ^2 could range from $\kappa^2 = 0$, for perpendicular alignment, to $\kappa^2 = 4$, for end-to-end parallel alignment.[47]

All three D−A1 assemblies are designed to form by hybridization of complementary tails appended to the cluster-nucleating templates. Prior work demonstrated that changes of just one base in a DNA strand can cause formation of different clusters.[48−51] Thus, appending a hybridization tail sequence to the cluster templating sequence could potentially destabilize the desired cluster in favor of other silver-DNA products. Because homopolymer strands of A and T bases do not form fluorescent clusters,[52] we chose to append complementary tails comprising mixed A and T sequences[23] to the D and A1 (or A2) cluster templating sequences. The calculated melting temperatures for these complementary tails are T_M = 42, 30, and 42 °C for the SC, DC, and EE assemblies, respectively.

Because the lengths of the templating sequences with appended tails exceed 50 bases, cluster sizes could not be determined using mass spectrometry (the propensity for DNA-salt associations results in poor ionization efficiencies and challenge mass spectrometry of long DNA strands).[53] Thus, to test whether the addition of hybridization tail and linker bases resulted in formation of differently structured clusters, we compared spectral properties of purified D and A clusters formed on only the template strands with properties of clusters formed on the template strands with appended tails. The strand alterations leave spectral properties of unhybridized D, A1 and A2 emitters unaltered (Supporting Information Figure S.3). Because the optical properties of few-atom silver clusters are sensitive to changes in cluster size of just one atom, as well as to cluster shape,[18,54,55] the lack of spectral changes with hybridization tails shows that the cluster structures are essentially unaltered.

The AT tails we append might still bind nonfluorescent silver products,[52] which could potentially hinder hybridization. To demonstrate that any such nonfluorescent clusters do not inhibit donor−acceptor binding, 10% native PAGE gels were run to compare D−A1 and D-A2 pairs with their respective monomer components. We additionally measured melting curves for hybridized pairs (Supporting Information Figure S.4) and found good agreement with calculated melting temperatures for the complementary tails. Measured melting temperatures for the SC and DC assemblies are $T_{M,meas}$ = 49 and 30 °C, respectively.

The hybridization was carried out with roughly a 2-fold excess of A-bearing cluster strands in order to minimize the presence of D clusters that are not incorporated into D−A pair assemblies. This is important because estimated FRET efficiencies, $E_{FRET} = 1 - I_{DA}/I_D$, are accurate only if the D−A pair solution contains no unhybridized D monomers and no hybridized assemblies with D clusters but not A clusters. The

pair solutions were prepared by mixing purified D and A components in 50 mM NH_4OAc at room temperature and incubating for 30 min. To remove unassembled donor strands that would mask FRET, hybridized solutions were then spin-filtered using 30 kDa centrifugal filters (Supporting Information, Figure S.5).

Figure 3 shows a representative gel shift assay of the double-clamp D−A1 pair solution. The purified D and A1 monomers and the D−A1 pair solution were run in lanes 1, 2, and 3, respectively. In the unstained gel (Figure 3a), UV excitation reveals the bands that contain fluorescent silver clusters, while SYBR gold staining (Figure 3b) shows all DNA products. The upper gel bands in the pair lanes confirm that hybridization formed the D−A assembly and that the D−A assembly is fluorescent (Figure 3a). The lower gel bands in lanes 3 that co-traveled with the unassembled cluster-bearing strands in lanes 1 and 2 show the additional presence of unassembled strands in the pair lane. This is likely due to partial melting of the assembled pair (T_M = 30 °C) by the heat generated during electrophoresis, though excess A1 cluster-bearing monomers that were not removed by spin filtering could also contribute.

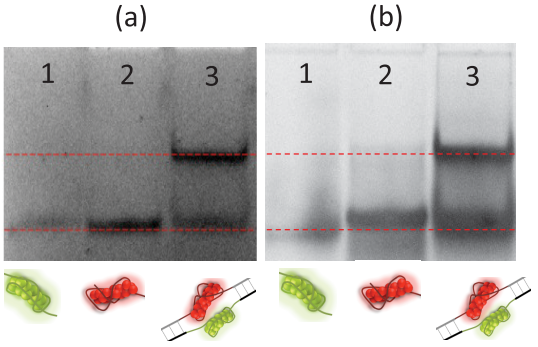

Figure 3. Gel shift assay of the silver cluster monomers and the double-clamp (DC) assembly. (a and b) Lane 1 contains the D cluster monomer, lane 2 contains the A1 cluster monomer, and lane 3 contains the D−A1 pair. The lower red lines mark the monomer bands and the upper red lines mark the DC assembly. (a) Unstained gel. The UV lightbox excites the fluorescent silver clusters in all lanes. (b) Stained gel.

The clear presence of D−A bands in the gel suggests that FRET should be observable in solution if SC and DC assembly designs do succeed in holding intact D and A clusters at separations comparable to R_0. Both SC and DC schemes (Figure 1) are expected to bring distinct Ag clusters within the 6 nm range and thus enable FRET. The EE design, however, separates D−A pairs by at least 10 nm, so in this case we expect negligible FRET.

Figure 4 shows emission contour plots for the single-clamp D and A1 monomers (Figure 4a,b) and hybridized single-clamp D−A1 solution (Figure 4c). The monomer emission spectra have been normalized by their respective concentrations relative to the spin-filtered D−A1 solution, as measured from the corresponding visible absorbance peaks (Supporting Information, Figure S.6),

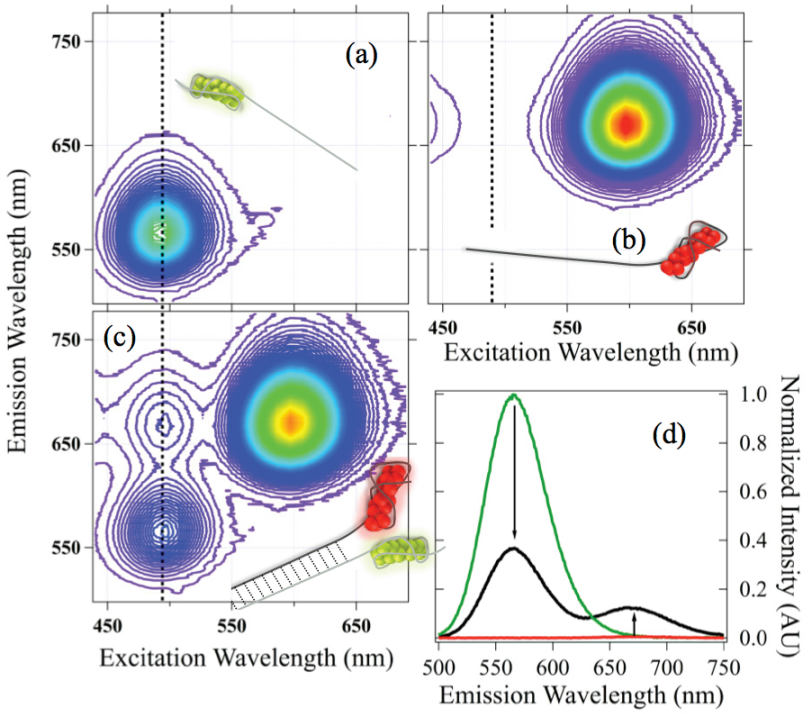

Figure 4. Inter-silver cluster FRET. (a) Fluorescence contour map for the 10 silver atom donor cluster, D. (b) Fluorescence contour map for the 15 silver atom acceptor cluster, A1. (c) Fluorescence contour map for D−A1 single clamp (SC) assembly. Acceptor emission appears at donor excitation wavelengths, a signature of FRET. (d) Data for 490 nm excitation (dotted line in (a)−(c)). Black line: emission spectrum of the D−A1 assembly. Green line: emission spectrum from D alone. Red line: emission spectrum from A1 alone. In the D−A1 SC and DC assemblies, FRET quenches the donor emission and dramatically increases the acceptor emission.

and all spectra have been normalized to the intensity of the Xe arc lamp used for excitation. Figure 4b shows that emission from the A1 monomer is not observed within the excitation range of the donor cluster (peak donor excitation is 490 nm, indicated by the dashed line). However, upon hybridization, excitation of the donor cluster produces emission from the A1 cluster, while simultaneously reducing donor emission (Figure 4c). These are unambiguous signatures of FRET.

Both of these phenomena are also clearly seen in the contour slice at the D cluster's maximum excitation wavelength, 490 nm (Figure 4d). Emission of the isolated donor (green line) is partially quenched in the hybridized construct (black line), while acceptor emission rises dramatically relative to the isolated A1 monomer (red line). Spectral characteristics for FRET displayed by SC (Figure 4) and DC (Supporting Information Figure S.7) D−A1 pairs demonstrate that D and A1 clusters are successfully brought within nanometer proximity. Similar spectra were observed for the SC D−A2 assembly (Supporting Information Figure S.8).

To confirm that the observed FRET signal does, in fact, result from strand hybridization and not an accidental transfer of one cluster onto the other strand, fluorescence from D−A1 pair solution was monitored during thermal cycling. Figure 5 shows representative thermal data for the D−A1 double clamp (DC) assembly, after correcting for the temperature dependence of the emission from D and A1 individually (Supporting Information Figure S.9). The melting point of the double-clamp assembly was determined to be $T_M \sim 30$ °C by monitoring absorbance at 260 nm as a function of temperature (Supporting Information Figure S.4).

Exciting D−A1 at 490 nm, we monitor both 670 nm emission intensity, corresponding to fluorescence from A1 (Figure 5a), and 560 nm emission intensity, corresponding to fluorescence from D (Figure 5b), as the temperature is cycled twice from 5 to 40 °C over a period of 80 min. At low temperatures, the FRET pairs are hybridized and 670 nm fluorescence from D−A1 is observed. As the temperature is increased past the melting point (indicated by black stars), 670 nm emission drops by roughly a factor of 7, which is significantly greater than the expected heating effects[56] for the A1 monomer (dashed blue trace, Figure 5a). We note that residual 670 nm emission is expected for the D−A1 pair at the maximum temperature of 40 °C due to incomplete melting of the hybridization tails.

The thermal modulation of 670 nm emission in D−A1 is anticorrelated with the temperature dependence of 560 nm emission from the donor cluster. At low temperatures, well below T_M, donor quenching by FRET produces lower intensity emission, while increasing T above T_M removes the FRET loss channel for the donor, resulting in brighter emission (Figure 5b).

As an additional control to confirm the correlation between strand hybridization and FRET, we performed

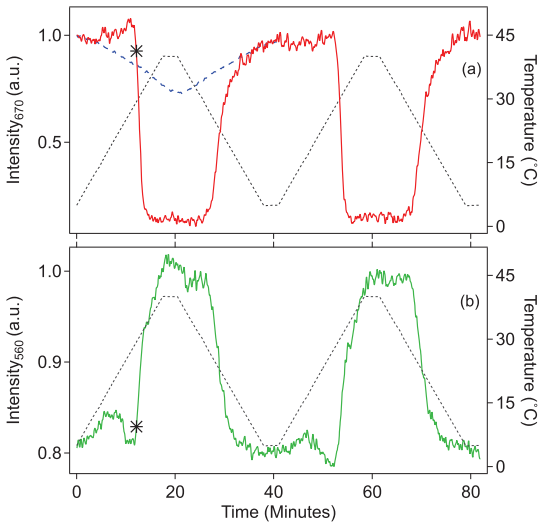

Figure 5. Fluorescence signals from (a) acceptor, with detection at 670 nm and (b) donor, with detection at 560 nm in the double clamp (DC) D−A1 pair, using 490 nm excitation, as the temperature is cycled twice from 5 to 40 °C (black dashed lines, right axes). Black stars indicate the melting temperature of the assembly as determined by A_{260} (Supporting Information Figure S.4). The blue dashed line (a) shows the temperature dependence of A1, using 600 nm excitation. Data were normalized to remove effects of photobleaching and temperature-dependent monomer brightness (Supporting Information Figure S.9).

the same experiment on D and A1 clusters formed on strands with *non*-complementary tails and did not observe FRET. The requirement for complementary tails and the observed intensity modulation around the hybridization melting point demonstrates that FRET pairs are indeed forming *via* strand hybridization.

The FRET efficiency varied among the three dual-cluster design schemes. As expected, the EE scheme produced no discernible FRET signal. This lack of FRET signal is reasonable because, with a cluster separation distance of 10 nm or more, the calculated FRET efficiency for this D−A1 pair in the EE scheme is 4% or less. FRET was observed for both SC and DC schemes. For the SC assembly, we used two normalization methods to determine the decrease in donor emission from the assembled D−A cluster pair solution relative to the D cluster monomer (Figure 4d, eq 3). The first method of normalizing relative concentrations involved using the ratio of 560 nm emission intensities from D monomer and SC D−A pair solutions at temperatures well above T_M, where there is no FRET quenching. These relative concentrations agreed well with those made using the second method, comparing the visible peak absorbance values at 490 nm in solutions of the D monomer alone and of D−A assemblies (Supporting Information Figure S.6). The two estimates from these methods yielded $E_{FRET} = 0.6-0.65$. For the DC assembly, we found $E = 0.6$ by again using the relative 560 nm intensities above T_m. These estimates of E_{FRET} from the partial quenching of donor emission provide a lower bound on the true FRET efficiency because the

possible presence of hybridized strands that lack an acceptor, or unhybridized strands containing only the donor cluster, will reduce the apparent FRET-induced quenching. We conclude that the SC and DC assemblies hold the D and A acceptors at separations within ~5–6 nm.

For comparison to inter-silver cluster FRET, we also studied a D–A pair in which the donor is an organic dye and the acceptor is a silver cluster. For this construct, the 3′ end of the DNA template sequence for silver cluster A1 was labeled with a donor Rhodamine (Rh) dye molecule, with peak excitation at 570 nm and peak emission at 590 nm. Four T bases were inserted between the dye and the template sequence to promote orientational averaging of the relative moment alignments of the dye and the cluster. The A1 cluster was synthesized directly on the Rh-labeled DNA and purified by HPLC.

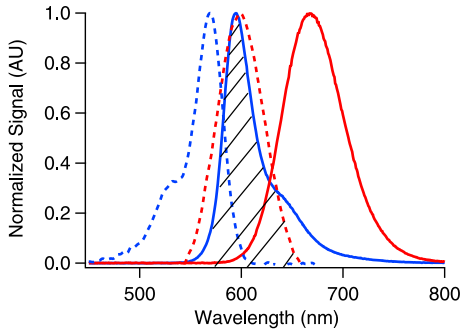

Figure 6. Blue traces show spectra of the Rh dye attached to the A1-templating DNA strand (without the A1 cluster). Red traces show spectra of the A1 silver cluster. Dashed lines are absorbance and solid lines are emission.

The characteristic vibronic sidebands of organic dye molecules are apparent for the Rh-labeled DNA in Figure 6 as the short wavelength shoulder in the absorbance and the long wavelength shoulder in the emission spectrum. These features are also apparent in the corresponding fluorescence contour map (Figure 7a). Such structure is strikingly absent in the corresponding spectra for the silver cluster synthesized on the DNA template alone (Figures 6 and 7b). This absence of vibronic structure in emission spectra from DNA-stabilized silver clusters is also a feature of individual silver clusters measured in the limit of very low temperatures (2 K), attesting to the clusters' metal–metal bonding character.[18]

Due to the vibronic shoulders on the Rh donor absorbance and emission spectra, the Rh–A1 spectra (Figure 7c,d) have a more complex appearance than for the dual silver cluster pair spectra (Figure 4). Nonetheless, we observe clear FRET signals from the Rh–A1 pair. From spectral characteristics of Rh and A1, we calculated R_0 to be 7.2 ± 0.2 nm, assuming $\kappa^2 = 2/3$. The decrease in donor emission gives $E_{FRET} \approx 67\%$ (a lower limit estimate since Rh-labeled DNA strands that do not hold a A1 cluster may also be present). For comparison, dye-based FRET studies of thymine homopolymer DNA strands with lengths of 10–40 bases found comparable FRET efficiencies at 18-base strand lengths,[57] after correcting for the smaller R_0 (6 nm) of the dye pair used in that study. Prior studies[18] indicated that the A1

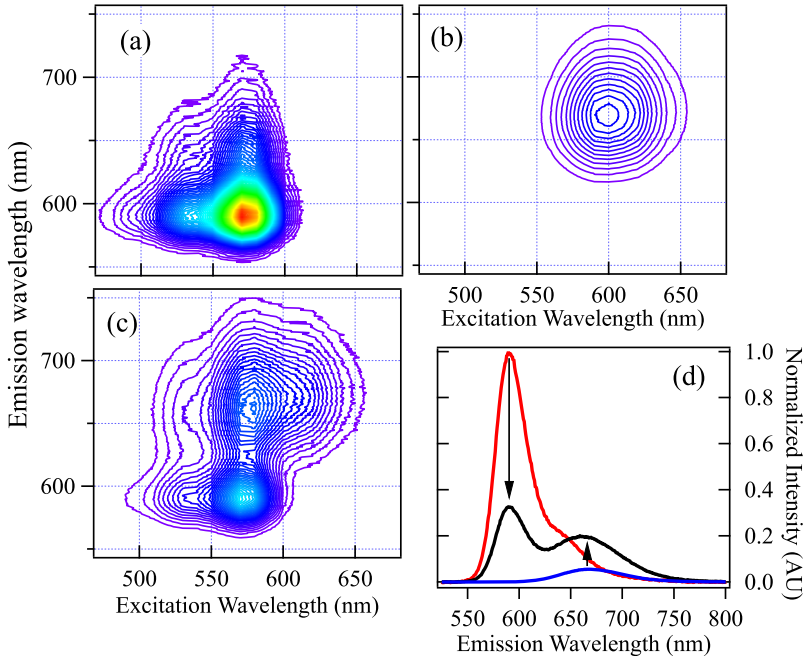

Figure 7. Rhodamine-silver cluster FRET. (a) Fluorescence contour map for the Rh donor dye, attached to the DNA strand. (b) Fluorescence contour map for the 15 silver atom acceptor cluster, A1, attached to the same DNA strand in (a), but with no dye. (c) Fluorescence contour map for Rh–A1 assembly. (d) Data for 570 nm excitation. Black line: Emission spectrum of the Rh–A1 assembly. Red line: emission spectrum from donor alone. Blue line: emission spectrum from acceptor alone. In the Rh–A1 assemblies, FRET quenches donor emission and dramatically increases acceptor emission.

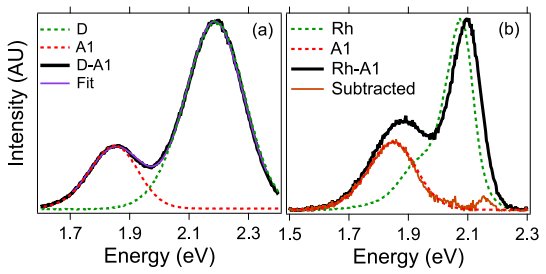

Figure 8. Analysis of the spectral stability of silver clusters in bicolor assemblies. Data are plotted *versus* energy to display lineshapes. (a) Black line: data for the SC dual silver cluster assembly. Green and red lines: data for D and A1 clusters. Purple line: dual Gaussian fit to dual cluster assembly data. The fitted wavelengths agree with those of the separate clusters to within 2 nm. (b) Black line: data for the Rhodamine–A1 pair. Green and red lines: Spectra of Rh dye only on the DNA strand and A1 cluster only on the templating DNA strand, respectively. Orange line: Data after subtracting a blue-shifted Rh spectrum overlie the spectrum of the A1 cluster.

cluster attaches to several bases within the 28-base DNA template, effectively making those bases part of the cluster itself. Thus ~18 bases is a reasonable overall length for the single-stranded DNA between the Rh dye molecule and the A1 cluster.

We now turn to the issue of the structural stability of the silver clusters. If assembly into dual cluster structures altered the number of silver atoms or significantly changed cluster shape, we would expect large spectral shifts in the spectra of D–A assemblies relative to those of individual clusters. Figure 8 shows that instead, the clusters in the bicolor assemblies exhibit the same spectral features as the individual clusters. To display the lineshapes, the emission data is plotted *versus* energy for the single clamp D–A1 assembly and its individual cluster components (Figure 8a) and for the Rh–A1 cluster assembly and components (Figure 8b). The D–A1 data can be fitted accurately by superposition of two Gaussians, with peak wavelengths that match those of the individual clusters within 2 nm. We conclude that the D and A clusters retain their individual structures when incorporated into nanometer-scale, dual-cluster assemblies.

For the Rh–A1 pair, the Rh dye peak shows a 6 nm blue-shift relative to the dye on the same DNA strand but without the cluster. To extract the spectrum of the A1 cluster, we subtracted a rigidly shifted dye spectrum. The resulting estimate of the cluster spectrum (orange line, Figure 8b) is nearly indistinguishable from that of the cluster alone (red dashed line). Apparently cluster formation affects the dye molecule fluorescence, perhaps due to altered dye-base pi stacking arising from changes in base orientation upon cluster formation. Variations in the spectral properties of Cy3, another commonly used fluorescent dye molecule, due to changes in the dye molecule's local environment, have also been demonstrated.[58] However, the silver cluster in the Rh–A1 assembly appears to be unchanged in the presence of the dye.

All results discussed thus far pertain to D–A pairs assembled from solutions of purified silver clusters. It would be desirable to create dual cluster constructs more simply, without purifying the individual silver cluster components. An obstacle to this approach is the heterogeneity of products produced by reduction of silver ions on DNA templates. To investigate the necessity of a purification stage, we attempted several different strategies to observe FRET without prepurification for the EE, DC and SC configurations using the silver clusters D and A1. These one- and two-pot methods rely instead on sufficient chemical yields of D and A1, with respect to other products, to result in a clear spectral signature of FRET. A summary of these attempts is in the Supporting Information. None results in any significant FRET signal, indicating insufficient chemical yields of the desired dual cluster assembly when using the D and A1 templates. When the relation between DNA sequence and cluster structure is better understood, it may become possible to select stabilizing templates that produce good yields of multicluster constructs without preliminary purification stages.

CONCLUSIONS

In conclusion, we have brought distinct silver nanoclusters, with sizes in the range of 10–20 atoms, into nanometer proximity. This was accomplished by using strand hybridization to merge distinct clusters of different size into nanoscale constructs. The success of the assemblies was verified using gel shift analyses and by monitoring FRET, an optical readout only occurring when donor–acceptor pairs are separated by just a few nanometers. To date, the FRET signatures are also temporally stable over times exceeding one month.

We find that both of the silver clusters participating in FRET preserve their spectral properties, indicating that each cluster maintains its original structure. The absence of vibronic structure in the cluster spectra simplifies the recognition of FRET features, relative to organic dyes. We find that Rhodamine is less spectrally stable upon assembly than the silver clusters themselves.

Prior studies of heterogeneous solutions produced by different template strands reported spectral changes upon altering the DNA environment. The structural stability we observe shows that appropriate strand selection results in clusters that are suitable for use in DNA-based nano-optical structures.

MATERIALS AND METHODS

Reagents and Synthesis. Samples were prepared by mixing DNA, NH_4OAc, and $AgNO_3$ (pH 7). Following a 20 min incubation at 4 °C, solutions were reduced with freshly prepared $NaBH_4$. For A1 and D, final concentrations were 15 μM DNA, 188 μM $AgNO_3$, 94 μM $NaBH_4$, and 10 mM NH_4OAc. For A2, final

concentrations were 5 μM DNA, 50 μM $AgNO_3$, 25 μM $NaBH_4$, and 10 mM NH_4OAc.

Oligonucleotides. The following strands (IDT, standard desalting) were used in the reported designs:

A1 (SC, EE): CACCGCTTTTGCCTTTTGGGGACGGATA-TTTTATT-AATAAATAATATTTAAAATTTATTATA

A1 (DC): AAAATTTATTATA-TTT-CACCGCTTTTGCCTTTTGGG-GACGGATA-TTT-ATTAATAAATAAT

D (SC): TATAATAAATTTTAAATATTATTTATTAAT-TTTT-TGCCTTTT-GGGGACGGATA

D (EE): TGCCTTTTGGGGACGGATA-TTTT-TATAATAAATTTT-AAATATTATTTATTAAT

D (DC): ATTATTTATTAAT-TTT-TGCCTTTTGGGGACGGATA-TTT-TATAATAAATTTT

A2 (SC): TTCCCACCCACCCCGGCCCGTT-TTTT-ATTAATAAA-TAATATTTAAAATTTATTATA

The A,T tails were previously reported in ref 23.

Purification. All silver-DNA solutions were purified using a Waters 2695 Separations Module with autoinjector and a Waters 2487 Dual Wavelength absorbance detector (10 μL volume), set to monitor the visible peak of each silver cluster. Separations used linear gradients from 15% to 35% of B (35 mM TEAA/MeOH[30]) with A (35 mM TEAA/H_2O[30]) on a 50 mm $\times$ 4.6 mm Kinetex C18 core–shell column with 2.6 μm particle size and 100 Å pore size (Phenomenex). Directly following HPLC purification, samples were dialyzed overnight into 50 mM NH_4OAc using 10 kDa MWCO MINI dialysis units (Thermo Scientific). The higher concentration buffer, relative to synthesis conditions, is used to promote hybridization of AT complementary tails.

Assembly. Purified components were mixed with an estimated 2-fold excess of A strands and spun in 10 kDa MWCO centrifugal filters (Millipore) to remove solvent and increase total DNA concentration to $\sim$1 μM. Solutions were left at room temperature for at least 30 min to allow complete hybridization. Hybridized solutions were then spun three times using 30 kDa centrifugal filters (Millipore) to remove excess monomers. Following each spin, buffer was added to ensure a final concentration of at least 50 mM NH_4OAc.

Calculated Melting Temperatures. Melting temperatures were calculated using 1 μM DNA and 50 mM Na^+ in the DINAMelt[59,60] web server. We use ammonium acetate rather than buffers containing Na^+, but prior work[61] has shown that equal concentrations of Na^+ and NH_4^+ ions give similar T_m results.

Conflict of Interest: The authors declare no competing financial interest.

Acknowledgment. This work was supported by NSF-CHE-0848375, NSF-CHE-1213895, STW-NWO Nano, and NSF-DGE-1144085 (NSF Fellowship, SC). We acknowledge use of the Biological Nanostructures Laboratory in the CNSI and MRL: an NSF MRSEC (DMR-1121053).

Supporting Information Available: Absorbance and fluorescence spectra for D–A2 SC pair; chromatograms and UV spectra of clusters in their template strands; D, A1 and A2 spectra with and without hybridization tails; melting curves for DC and SC assemblies; FRET data before and after centrifugal filtration; absorbance spectra of D–A1 monomers and pair; FRET data for D–A1 DC and D–A2 SC pairs; normalization for Figure 5; *E* from D emission brightness above T_M; discussion of attempts to assemble D–A1 pairs without a monomer purification step. This material is available free of charge *via* the Internet at http://pubs.acs.org.

REFERENCES AND NOTES

1. Kuzyk, A.; Schreiber, R.; Fan, Z.; Pardatscher, G.; Roller, E.-M.; Högele, A.; Simmel, F. C.; Govorov, A. O.; Liedl, T. DNA-Based Self-Assembly of Chiral Plasmonic Nanostructures with Tailored Optical Response. *Nature* **2012**, *483*, 311–314.
2. Ding, B.; Deng, Z.; Yan, H.; Cabrini, S.; Zuckermann, R. N.; Bokor, J. Gold Nanoparticle Self-Similar Chain Structure Organized by DNA Origami. *J. Am. Chem. Soc.* **2010**, *132*, 3248–3249.
3. Pal, S.; Deng, Z.; Wang, H.; Zou, S.; Liu, Y.; Yan, H. DNA Directed Self-Assembly of Anisotropic Plasmonic Nanostructures. *J. Am. Chem. Soc.* **2011**, *133*, 17606–17609.
4. Yao, H.; Yi, C.; Tzang, C.-H.; Zhu, J.; Yang, M. DNA-Directed Self-Assembly of Gold Nanoparticles into Binary and Ternary Nanostructures. *Nanotechnology* **2007**, *18*, 015102.
5. Aldaye, F. A.; Sleiman, H. F. Sequential Self-Assembly of a DNA Hexagon as a Template for the Organization of Gold Nanoparticles. *Angew. Chem., Int. Ed.* **2006**, *45*, 2204–2209.
6. Gaiduk, A.; Yorulmaz, M.; Orrit, M. Correlated Absorption and Photoluminescence of Single Gold Nanoparticles. *ChemPhysChem* **2011**, *12*, 1536–1541.
7. Buttet, J.; Félix, C.; Harbich, W.; Rabin, I. Ag8 Fluorescence in Argon. *Phys. Rev.* **2001**, *86*, 2992–2995.
8. Shang, L.; Dong, S.; Nienhaus, G. U. Ultra-Small Fluorescent Metal Nanoclusters: Synthesis and Biological Applications. *Nano Today* **2011**, *6*, 401–418.
9. Díez, I.; Ras, R. H. Fluorescent Silver Nanoclusters. *Nanoscale* **2011**, *3*, 1963–1970.
10. Zheng, J.; Dickson, R. M. Individual Water-Soluble Dendrimer-Encapsulated Silver Nanodot Fluorescence. *J. Am. Chem. Soc.* **2002**, *124*, 13982–13983.
11. Yu, J.; Patel, S. A.; Dickson, R. M. *In Vitro* and Intracellular Production of Peptide-Encapsulated Fluorescent Silver Nanoclusters. *Angew. Chem.* **2007**, *119*, 2074–2076.
12. Xu, H.; Suslick, K. S. Sonochemical Synthesis of Highly Fluorescent Ag Nanoclusters. *ACS Nano* **2010**, *4*, 3209–3214.
13. Cathcart, N.; Mistry, P.; Makra, C.; Pietrobon, B.; Coombs, N.; Jelokhani-Niaraki, M.; Kitaev, V. Chiral Thiol-Stabilized Silver Nanoclusters with Well-Resolved Optical Transitions Synthesized by a Facile Etching Procedure in Aqueous Solutions. *Langmuir* **2009**, *25*, 5840–5846.
14. Cathcart, N.; Kitaev, V. Silver Nanoclusters: Single-Stage Scaleable Synthesis of Monodisperse Species and Their Chirooptical Properties. *J. Phys. Chem. C* **2010**, *114*, 16010–16017.
15. Adhikari, B.; Banerjee, A. Facile Synthesis of Water-Soluble Fluorescent Silver Nanoclusters and HgII Sensing. *Chem. Mater.* **2010**, *22*, 4364–4371.
16. Ledo-Suárez, A.; Rivas, J.; Rodríguez-Abreu, C. F.; Rodríguez, M. J.; Pastor, E.; Hernández-Creus, A.; Oseroff, S. B.; López-Quintela, M. A. Facile Synthesis of Stable Subnanosized Silver Clusters in Microemulsions. *Angew. Chem., Int. Ed.* **2007**, *46*, 8823–8827.
17. Petty, J. T.; Zheng, J.; Hud, N. V.; Dickson, R. M. DNA-Templated Ag Nanocluster Formation. *J. Am. Chem. Soc.* **2004**, *126*, 5207–5212.
18. Schultz, D.; Gardner, K.; Oemrawsingh, S. S. R.; Markešević, N.; Olsson, K.; Debord, M.; Bouwmeester, D.; Gwinn, E. Evidence for Rod-Shaped DNA-Stabilized Silver Nanocluster Emitters. *Adv. Mater.* **2013**, *25*, 2797–2803.
19. Sharma, J.; Yeh, H.-C.; Yoo, H.; Werner, J. H.; Martinez, J. S. A Complementary Palette of Fluorescent Silver Nanoclusters. *Chem. Commun.* **2010**, *46*, 3280.
20. Liu, X.; Atwater, M.; Wang, J.; Huo, Q. Extinction Coefficient of Gold Nanoparticles with Different Sizes and Different Capping Ligands. *Colloids Surf., B* **2007**, *58*, 3–7.
21. Baishya, K.; Idrobo, J.; Öğüt, S.; Yang, M.; Jackson, K.; Jellinek, J. Optical Absorption Spectra of Intermediate-Size Silver Clusters From First Principles. *Phys. Rev. B* **2008**, *78*, 075439.
22. Harb, M.; Rabilloud, F.; Simon, D. Optical Absorption of Silver Clusters: A Study of the Effective Potential Core Size. *Chem. Phys. Lett.* **2009**, *476*, 186–190.
23. Yeh, H. C.; Sharma, J.; Han, J. J.; Martinez, J. S.; Werner, J. H. A DNA–Silver Nanocluster Probe That Fluoresces Upon Hybridization. *Nano Lett.* **2010**, *10*, 3106–3110.
24. Huang, Z.; Tao, Y.; Pu, F.; Ren, J.; Qu, X. Versatile Logic Devices Based on Programmable DNA-Regulated Silver-Nanocluster Signal Transducers. *Chem.—Eur. J.* **2012**, *18*, 6663–6669.
25. Shah, P.; Rørvig-Lund, A.; Chaabane, S. B.; Thulstrup, P. W.; Kjaergaard, H. G.; Fron, E.; Hofkens, J.; Yang, S. W.; Vosch, T. Design Aspects of Bright Red Emissive Silver Nanoclusters/DNA Probes for MicroRNA Detection. *ACS Nano* **2012**, *6*, 8803–8814.

26. Yang, S. W.; Vosch, T. Rapid Detection of MicroRNA by a Silver Nanocluster DNA Probe. *Anal. Chem.* **2011**, *83*, 6935–6939.
27. Zhang, L.; Zhu, J.; Guo, S.; Li, T.; Li, J.; Wang, E. Photoinduced Electron Transfer of DNA/Ag Nanoclusters Modulated by G-Quadruplex/Hemin Complex for the Construction of Versatile Biosensors. *J. Am. Chem. Soc.* **2013**, *135*, 2403–2406.
28. Li, T.; Zhang, L.; Ai, J.; Dong, S.; Wang, E. Ion-Tuned DNA/Ag Fluorescent Nanoclusters as Versatile Logic Device. *ACS Nano* **2011**, *5*, 6334–6338.
29. Gwinn, E. G.; O'Neill, P.; Guerrero, A. J.; Bouwmeester, D.; Fygenson, D. K. Sequence-Dependent Fluorescence of DNA-Hosted Silver Nanoclusters. *Adv. Mater.* **2008**, *20*, 279–283.
30. Petty, J. T.; Fan, C.; Story, S. P.; Sengupta, B.; Sartin, M.; Hsiang, J.-C.; Perry, J. W.; Dickson, R. M. Optically Enhanced, Near-IR, Silver Cluster Emission Altered by Single Base Changes in the DNA Template. *J. Phys. Chem. B* **2011**, *115*, 7996–8003.
31. Han, B.; Wang, E. DNA-Templated Fluorescent Silver Nanoclusters. *Anal. Bioanal. Chem.* **2011**, *402*, 129–138.
32. Driehorst, T.; O'Neill, P.; Goodwin, P. M.; Pennathur, S.; Fygenson, D. K. Distinct Conformations of DNA-Stabilized Fluorescent Silver Nanoclusters Revealed by Electrophoretic Mobility and Diffusivity Measurements. *Langmuir* **2011**, *27*, 8923–8933.
33. Rothemund, P. W. K. Folding DNA to Create Nanoscale Shapes and Patterns. *Nature* **2006**, *440*, 297–302.
34. Ke, Y.; Ong, L. L.; Shih, W. M.; Yin, P. Three-Dimensional Structures Self-Assembled From DNA Bricks. *Science* **2012**, *338*, 1177–1183.
35. Dietz, H.; Douglas, S. M.; Shih, W. M. Folding DNA Into Twisted and Curved Nanoscale Shapes. *Science* **2009**, *325*, 725–730.
36. Douglas, S. M.; Dietz, H.; Liedl, T.; Högberg, B.; Graf, F.; Shih, W. M. Self-Assembly of DNA Into Nanoscale Three-Dimensional Shapes. *Nature* **2009**, *459*, 414–418.
37. Vosch, T.; Antoku, Y.; Hsiang, J. C.; Richards, C. I.; Gonzalez, J. I.; Dickson, R. M. Strongly Emissive Individual DNA-Encapsulated Ag Nanoclusters as Single-Molecule Fluorophores. *Proc. Natl. Acad. Sci. U.S.A.* **2007**, *104*, 12616–12621.
38. Oemrawsingh, S. S. R.; Markešević, N.; Gwinn, E. G.; Eliel, E. R.; Bouwmeester, D. Spectral Properties of Individual DNA-Hosted Silver Nanoclusters at Low Temperatures. *J. Phys. Chem. C* **2012**, *116*, 25568–25575.
39. O'Neill, P. R.; Young, K.; Schiffels, D.; Fygenson, D. K. Few-Atom Fluorescent Silver Clusters Assemble at Programmed Sites on DNA Nanotubes. *Nano Lett.* **2012**, *12*, 5464–5469.
40. de Heer, W. A. The Physics of Simple Metal Clusters: Experimental Aspects and Simple Models. *Rev. Mod. Phys.* **1993**, *65*, 611–676.
41. Gutierrez, M.; Henglein, A. Formation of Colloidal Silver by" Push-Pull" Reduction of Silver (1+). *J. Phys. Chem.* **1993**, *97*, 11368–11370.
42. Sharma, J.; Yeh, H.-C.; Yoo, H.; Werner, J. H.; Martinez, J. S. Silver Nanocluster Aptamers: *In Situ* Generation of Intrinsically Fluorescent Recognition Ligands for Protein Detection. *Chem. Commun.* **2011**, *47*, 2294–2296.
43. Yeh, H. C.; Sharma, J.; Shih, I. M.; Vu, D. M.; Martinez, J. S.; Werner, J. H. A Fluorescence Light-Up Ag Nanocluster Probe That Discriminates Single-Nucleotide Variants by Emission Color. *J. Am. Chem. Soc.* **2012**, *134*, 11550–11558.
44. Förster, T. 10th Spiers Memorial Lecture. Transfer Mechanisms of Electronic Excitation. *Discuss. Faraday Soc.* **1959**, *27*, 7–17.
45. Förster, T. Zwischenmolekulare Energiewanderung Und Fluoreszenz. *Ann. Phys* **1948**, *437*, 55–75.
46. Schultz, D.; Gwinn, E. G. Silver Atom and Strand Numbers in Fluorescent and Dark Ag:DNAs. *Chem. Commun.* **2012**, *48*, 5748–5750.
47. Clegg, R. M. Fluorescence Resonance Energy Transfer and Nucleic Acids. *Methods Enzymol.* **1992**, *211*, 353–388.
48. Guo, W.; Yuan, J.; Dong, Q.; Wang, E. Highly Sequence-Dependent Formation of Fluorescent Silver Nanoclusters in Hybridized DNA Duplexes for Single Nucleotide Mutation Identification. *J. Am. Chem. Soc.* **2010**, *132*, 932–934.
49. Cui, Q.; Ma, K.; Shao, Y.; Xu, S.; Wu, F.; Liu, G.; Teramae, N.; Bao, H. Gap Site-Specific Rapid Formation of Fluorescent Silver Nanoclusters for Label-Free DNA Nucleobase Recognition. *Anal. Chim. Acta* **2012**, *724*, 86–91.
50. Ma, K.; Cui, Q.; Liu, G.; Wu, F.; Xu, S.; Shao, Y. DNA Abasic Site-Directed Formation of Fluorescent Silver Nanoclusters for Selective Nucleobase Recognition. *Nanotechnology* **2011**, *22*, 305502.
51. Zhang, M.; Guo, S.-M.; Li, Y.-R.; Zuo, P.; Ye, B.-C. A Label-Free Fluorescent Molecular Beacon Based on DNA-Templated Silver Nanoclusters for Detection of Adenosine and Adenosine Deaminase. *Chem. Commun.* **2012**, *48*, 5488–5490.
52. Schultz, D.; Gwinn, E. Stabilization of Fluorescent Silver Clusters by RNA Homopolymers and Their DNA Analogs: C, G *versus* A, T (U) Dichotomy. *Chem. Commun* **2011**, *47*, 4715–4717.
53. Potier, N.; Van Dorsselaer, A.; Cordier, Y.; Roch, O.; Bischoff, R. Negative Electrospray Ionization Mass Spectrometry of Synthetic and Chemically Modified Oligonucleotides. *Nucleic Acids Res.* **1994**, *22*, 3895–3903.
54. Johnson, H. E.; Aikens, C. M. Electronic Structure and TDDFT Optical Absorption Spectra of Silver Nanorods. *J. Phys. Chem. A* **2009**, *113*, 4445–4450.
55. Guidez, E. B.; Aikens, C. M. Theoretical Analysis of the Optical Excitation Spectra of Silver and Gold Nanowires. *Nanoscale* **2012**, *4*, 4190.
56. Guo, W.; Orbach, R.; Mironi-Harpaz, I.; Seliktar, D.; Willner, I. Fluorescent DNA Hydrogels Composed of Nucleic Acid-Stabilized Silver Nanoclusters. *Small* **2013**, 10.1002/smll.201300055.
57. Murphy, M. C.; Rasnik, I.; Cheng, W.; Lohman, T. M.; Ha, T. Probing Single-Stranded DNA Conformational Flexibility Using Fluorescence Spectroscopy. *Biophys. J.* **2004**, *86*, 2530–2537.
58. Iqbal, A.; Arslan, S.; Okumus, B.; Wilson, T. J.; Giraud, G.; Norman, D. G.; Ha, T.; Lilley, D. M. Orientation Dependence in Fluorescent Energy Transfer Between Cy3 and Cy5 Terminally Attached to Double-Stranded Nucleic Acids. *Proc. Natl. Acad. Sci. U.S.A.* **2008**, *105*, 11176–11181.
59. Markham, N. R.; Zuker, M. DINAMelt Web Server for Nucleic Acid Melting Prediction. *Nucleic Acids Res.* **2005**, *33*, W577–W581.
60. Markham, N. R.; Zuker, M. UNAFold: Software for Nucleic Acid Folding and Hybridization. *Methods Mol. Biol.* **2008**, *453*, 3–31.
61. Stellwagen, E.; Muse, J. M.; Stellwagen, N. C. Monovalent Cation Size and DNA Conformational Stability. *Biochemistry* **2011**, *50*, 3084–3094.